N68-37712 02

N68-37712 C1

LUNAR LANDING MODULE REFLECTIVITY MODEL*

By

A. Tong and H. S. Hayre

TR-67-14

CULLEN COLLEGE OF ENGINEERING

UNIVERSITY OF HOUSTON

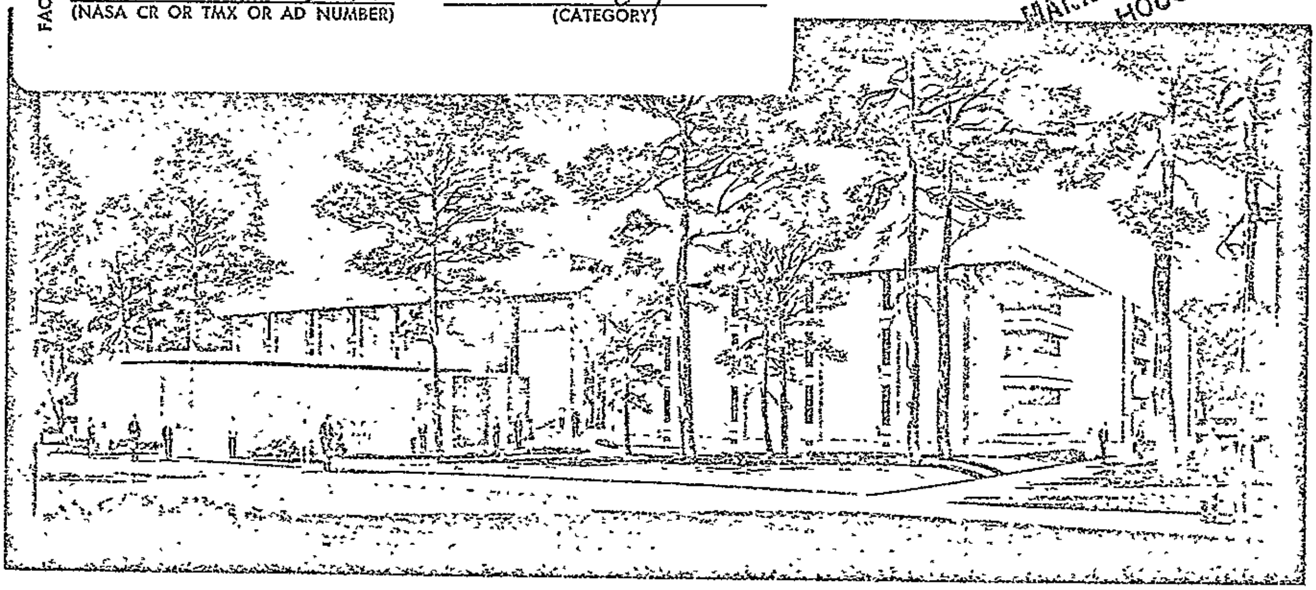

HOUSTON, TEXAS

CASE FILE COPY

NASA CR 92342

LUNAR LANDING MODULE REFLECTIVITY MODEL*

By

A. Tong and H. S. Hayre

TR-67-14

Wave Propagation Laboratory
Department of Electrical Engineering

UNIVERSITY OF HOUSTON
Cullen College of Engineering
Cullen Boulevard
Houston, Texas 77004

August, 1967

*This work is sponsored by NASA - Manned Spacecraft Center, under Contract NAS-9-6760.

ABSTRACT

Previous lunar surface models consisted of randomly varying surface heights with isotropic surface height spatial correlation functions or sectional correlation functions or some other surface slope distribution. Furthermore, a superposition of various types of surfaces such as small and large scale roughness were also employed. These models do not seem to represent explicitly the lunar craters which are superimposed on the random height variations. It is this aspect of rimmed craters superimposed on a two dimensional distribution of surface heights with each component surface being a random variable but statistically independent of each other, that is used to calculate the monostatic radar return for the Lunar Landing Module guidance and control radars at various angles of incidence. The unique feature of this surface model is that a random variation of the spacing between the rimmed craters allows a realistic spatial distribution as well as size distribution which has been found to be exponential from Orbitor I and II photographic data of medium and fine resolutions. The near-vertical incidence radar return power is calculated using scalar Helmholtz integral and the results are then reduced to a few special cases such as one generated when the randomly varying main crater diameter tends to zero and the

random period or distance between crater centers tends to infinity. The results seem to indicate that this model may be used to generate a wide variety of randomly rough surfaces for a calculation of their radar return.

TABLE OF CONTENTS

LIST OF FIGURES

CHAPTER I

INTRODUCTION

An electromagnetic wavefront incident on an obstacle induces a charge thereon which causes each point on its surface to radiate secondary waves in all directions. Each point acts as a Huygens source and this phenomena is termed scattering, and physical optic techniques may be used in order to analyze the scattering. The re-radiation from a surface illuminated by an electromagnetic wavefront depends on such surface properties as its permittivity, permeability and conductivity. In theory, a complete knowledge of the surface parameters and its roughness would yield its scattering pattern for a given source of the incident energy, although the calculation procedure is very complicated in the case of a randomly rough surface. Therefore, certain assumptions given below must be made to simplify the mathematical manipulation and to ensure the validity of the resulting solution.

a) The incident wave is monochromatic

b) The polarization of the incident wave is linear

c) The distance between the source and the reflecting surface is large compared to the surface dimension, so that the wavefront may be treated as a plane wave, and

d) The edge effect, shadowing, and multiple scattering are assumed negligible.

In spite of these restrictions and assumptions, a complete solution of the problem of scattering has not been found as yet although considerable work has been done in the area by physicists and engineers for the last twenty-five years.

Theoretically, a terrain may be thought of as a randomly spaced array of scatterers which yield a certain radar scattering pattern, and conversely, knowing the scattering pattern, an unknown terrain may be specified. This technique of surface roughness detection by employing radar backscattering cross-section has attracted considerable interest in recent years.

The terrain illuminated by a radar is quite often randomly rough, therefore it is necessary to use probability techniques in its description; consequently, the radar return obtained from it is also described statistically. The present investigation of the lunar surface radar return assumes that it is a perfectly conducting surface at high frequencies. The Fresnel reflection coefficient for horizontally polarized plane wave is

$$R = \frac{\cos\theta - \sqrt{\gamma^2 - \sin^2\theta}}{\cos\theta + \sqrt{\gamma^2 - \sin^2\theta}} \tag{1-1}$$

where θ is the local angle of incidence and

$$\gamma = \sqrt{\frac{\frac{\epsilon}{\epsilon_0} + i\,60\lambda\sigma}{\frac{\mu}{\mu_0} + i\frac{k_m}{\mu_0}}} \tag{1-2}$$

as shown in Fig. 1-1, where various terms are defined. For a perfectly conducting surface, ϵ and γ are infinite and

$$R = -1. \tag{1-3}$$

The early lunar models were based on the earth-based lunar radar echoes, and some investigators such as Senior and Siegel (1959) regarded the moon as a quasi-smooth scatterer. A hypothetical surface model consisting of corner reflectors, cone-like projections of small included angle, and flat areas, was also used by them to calculate the radar scattering cross-section, employing an approximate theoretical form of the power reflection coefficient.

Katz and Spetner (1960) presented two statistical models of rough surfaces, namely the Specular-Point and Random-Scatterer model. In the Specular-Point model, the rough surface was assumed to be a perfect conductor and the surface height function was assumed to be not only continuous but also to have continuous derivatives with gaussian distribution of surface slopes. The radar return from the surface was supposed to be predominantly contributed by large facets oriented perpendicular to the incident radiation, and remaining contributions coming from small isotropic scatterers.

In the Random-Scatterer model, the radar return was assumed to be generated mainly by a large number of

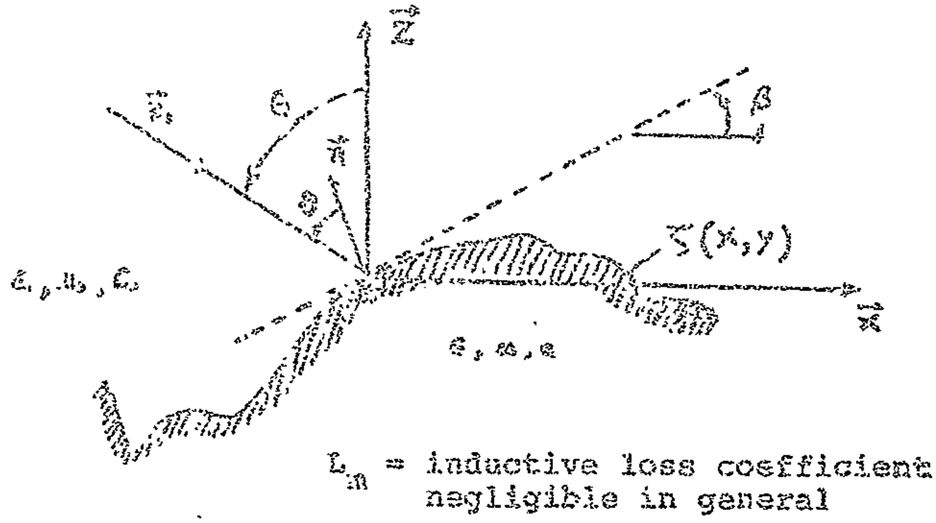

Fig. 1-1. The Local Scattering Geometry. ($\vec{n}$ is the local normal. ϑ is the local angle of incidence and ϑ_1 is the overall angle of incidence defined with respect to $\hat{z}$.)

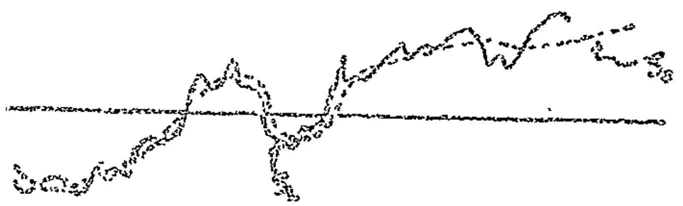

Fig. 1-2. A Rough Surface Composed of Small-Scale ζ_s and Large-Scale Roughness ζ_L.

statistically independent and incoherent scatterers, such as a random array of corner reflectors, distributed upon a non-reflecting plane surface.

Brown (1960) assumed the lunar radar echo to be made up of specular and Lambert scatter components. And the lunar surface was interpreted to be made up of two parts, one consisting of a statistical array of mirror-like reflectors having exponential probability density function and cuasing the specular return component and the random roughness contributing to the Lambert scatter component of the return power.

Hayre (1962) used a lunar model which consists of randomly varying surface heights (gaussian density function), surface slope distribution and the height-distance autocovariance function which were calculated for various terrains. These statistical functions are considered to describe a rough surface sufficiently well. Later in 1965, Hayre, based on the above statistical parameters, suggested a composite roughness to describe the lunar surface. The superposition model considers a slowly varying large-scale roughness and a rapidly varying small-scale roughness within the limits of the validity of the Kirchhoff integral approach, and it is assumed that they are correlated (Fig. 1-2). The interdependency of the two rough profiles seems to represent a surface model in a very realistic manner.

A review of the lunar models of the past indicates that they were good estimates of the lunar surface roughness, as interpreted from the earth-based radar lunar echoes. However, these cannot represent such lunar surface features as craters and their rims for the LM radar reflectivity calculations.

The requirement of a high degree of accuracy in calculation of radar signal degradation by the lunar surface initiated the formulation of a new lunar model, which is discussed later. The flexibility and general nature of the model components and their statistical parameters suggested the use of the same approach for a description of many other rough features. Finally, a mathematical solution for the average radar return power including the lunar surface effects is presented.

CHAPTER II

LUNAR SURFACE MODELING

The Apollo guidance and control signals during landing are primarily conditioned by the lunar surface roughness. An accurate analysis of lunar surface roughness in the radar-echo study provides the means to predict the effects of the former on the guidance and control commands which are generated by a computer on board the module after processing the radar return signals from the velocity and altimeter radars. The lunar surface roughness is expected to bias the lunar landing module (LM) radar signals used for guidance and control during its landing. It is this aspect of lunar radar echo-degradation of LM velocity and altimeter beams which is discussed in this paper.

Although the early scientific efforts had provided valuable information on surface roughness of the moon, the application of their data was limited for various reasons including the lack of full scale verification. Even the recently acquired earth-based radar information about the lunar surface was not sufficiently detailed, partly due to the libration of the moon and partly due to the fading caused by the inhomogeneous ionospheric medium.

The availability of a high-energy source for a high-frequency radar was in itself a problem. Consequently, radar observations could not supply reliable evidence on the nature of the lunar surface structures of the order of a meter or smaller in dimensions. For example, according to Hayre's criterion (1961), a random rough surface is considered smooth for vertical incidence if

$$\sigma \leq \frac{\lambda}{12} \qquad (2-1)$$

where

σ is the standard deviation of the surface undulation in meters, and

λ is the incident wavelength in meters.

If λ is 4 meters, a surface with a standard deviation of 0.3 meters is considered smooth. As a result, only the large scale roughness features could be obtained from the lunar radar echoes.

In 1961, Hayre and Moore conducted a laboratory experiment and accoustically simulated the lunar echoes. Nonlinear acoustic modeling techniques were used to model the lunar surface on a set of scaled down aluminum spheres. The acoustic return data was used to formulate a statistical model composed of a large-scale roughness and small-scale roughness with their reasonably complete statistical description including cross-correlation between these two components. The general Kirchhoff's solution with its usual assumptions was used in their theoretical model to obtain a mathematically manageable expression for radar cross-section. However, their model was not designed to describe such irregular and nonuniform surface features as lunar ridges in general, and craters and rims in particular.

Some other attempts have been made to model the lunar backscatter cross-section (Mayre, 1962, Muehlman, 1966). Muehlman based his results on two point radar data from Surveyor I. The simplified radar scattering cross-section equation includes weighted statistical parameters of the lunar surface such as standard deviation, the decorrelation constant and incident angle. Recent U. S. Ranger, Surveyors, and Orbiter I and II photographs of the surface of the moon show it to contain nonuniform roughness with its statistics varying from region to region. Thus, these previous models do not suffice for this study of degradation of radar signals for guidance systems of Apollo landing.

With the advent of the successive Orbiter missions, more detailed lunar surface photographs have now been obtained. Information extracted from the Orbiter photographs and their mosaic overlays is believed to be sufficiently complete to establish a set of roughness parameters corresponding to each particular lunar site. These parameters are the large-scale and small-scale random roughness, crater-size probability distribution with inter-relationship among the crater dimensions, such as the diameter, depth and rim height and rim base width. Mosaic surface data from a number of preselected LM landing sites have been carefully analyzed and their roughness parameters seem to be statistically independent from one site to the next. Therefore, a surface model composed of uncorrelated random and periodic structure with random or fixed parameters is formulated.

The present model is a superposition of a gaussian random rough surface, and a periodic crater outline surface which can be made random as well. The random surface $\xi_R(x,y)$ is assumed to have a mean value of zero and variance of σ as shown in Fig. 2-1. Its autocorrelation function is assumed to be $\exp\frac{-|\tau|}{B}$ (Hayre, 1961) where τ is the distance between two points measured on the X-Y plane, and B is the decorrelation distance. The periodic surface $\xi_p(x,y)$ is defined differently over three zones within a typical interval, as shown in Fig. 2-2 and 2-3.

In Zone I

$$\xi_p(x,y) = 0 \qquad \text{for } x^2+y^2 > d_2^2 \qquad (2\text{-}2)$$

In Zone II

$$\xi_p(x,y) = h_2 \sin\frac{\pi(\sqrt{x^2+y^2}-d_1)}{d_2-d_1} \qquad \text{for } d_1^2 < x^2+y^2 < d_2^2 \qquad (2\text{-}3)$$

In Zone III

$$\xi_p(x,y) = -h_1 \cos\frac{\pi\sqrt{x^2+y^2}}{2d_1} \qquad \text{for } x^2+y^2 < d_1^2 \qquad (2\text{-}4)$$

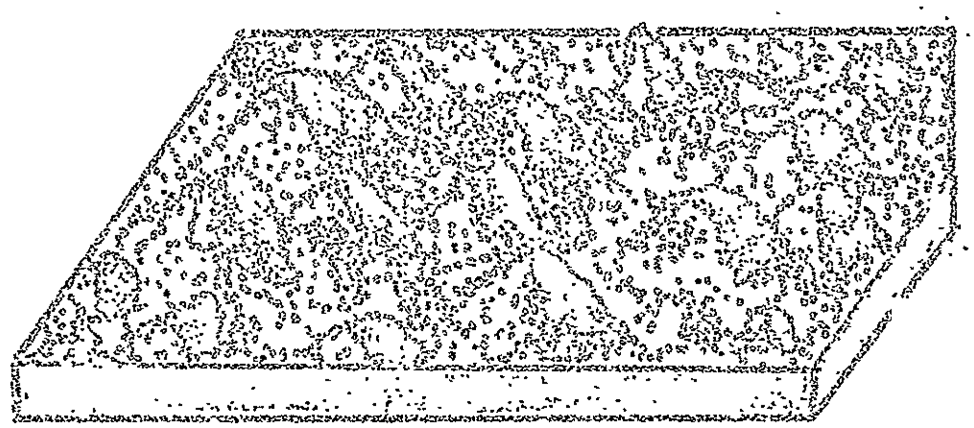

Three-Dimensional Representation

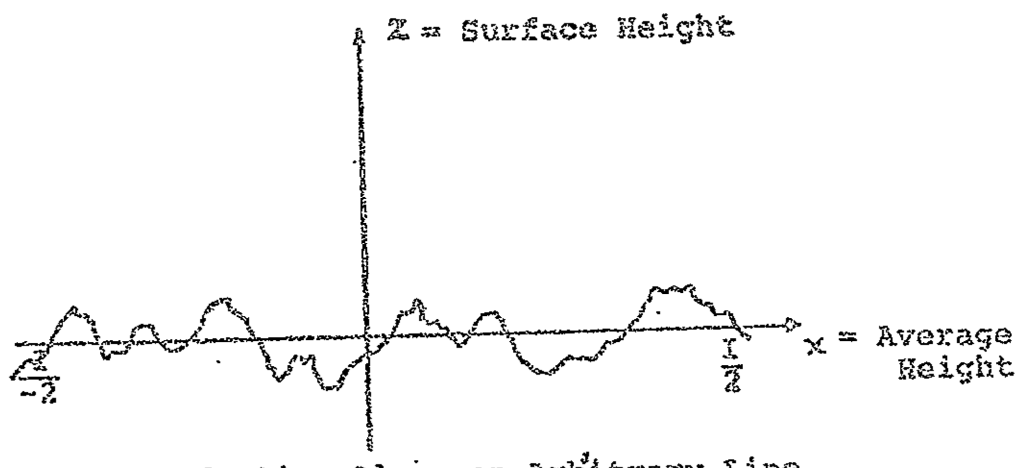

Profile Cross-Section Along an Arbitrary Line.

Fig. 2-1. A Random Surface Component.

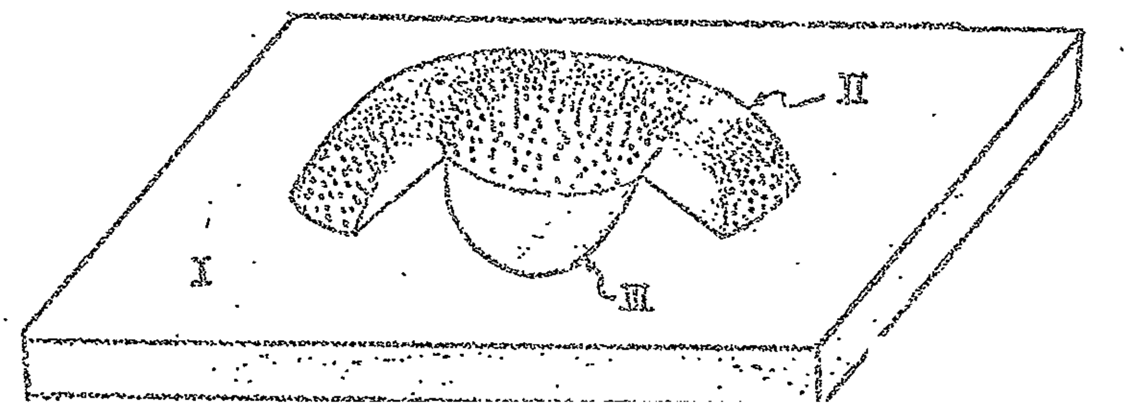

Fig. 2-2. A Periodic Surface Component

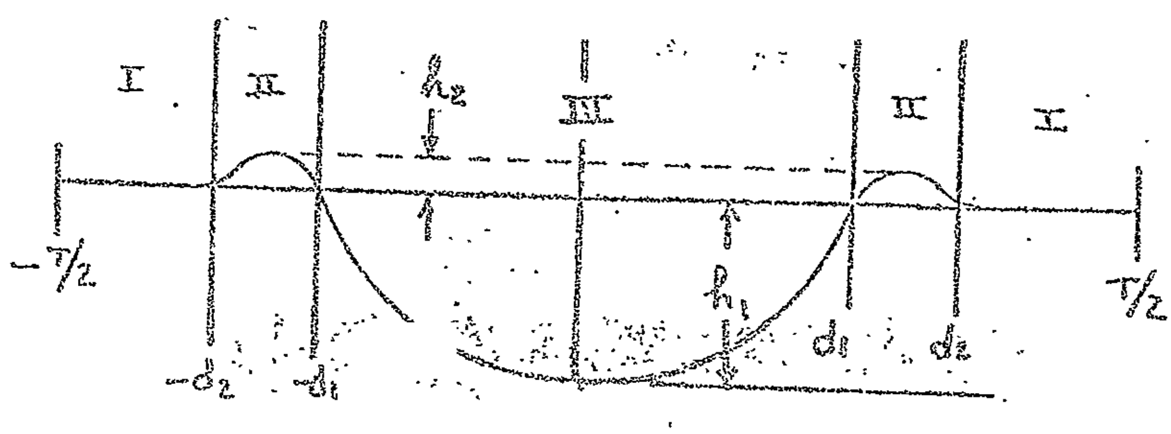

Fig. 2-3. A Cross-Section View of the Periodic Surface

The component ξ_R represents the general small-scale or large-scale roughness, while the component ξ_P may be designed to represent craters, boulders, and hills. An appropriate selection of the variables d_1, d_2, h_1, and h_2, and the combination of ξ_R and ξ_P may be devised to fit the description of most types of lunar surface features. For instance, by varying σ/λ and β/λ, ξ_R may be varied from smooth to a very rough surface.

If h_1 and h_2 approach zero, the surface ξ_P becomes mirror-like. Similarly, a suitable choice of h_1, h_2, d_1, and d_2 may be made to represent most surface rills and protrusions. The flexibility of this particular model in terms of functions ξ_R and ξ_P renders a manipulable means for mathematical calculation of radar return signals.

The quasi-periodic component ξ_P may assume any geometrical function which is most appropriate for the terrain description in keeping with the assumption of negligible shadowing and multiple reflections, etc. A careful analysis of the Orbiters' high resolution photographic mosaics indicates that the sinusoidal surface function very nearly matches the description of the lunar surface. The sinusoidal function is superior geometrically and flexible mathematically. For example, the function

$$\xi(x) = h \sin \frac{\pi x}{r} \qquad (2-5)$$

where

h = the surface height, and

T = the surface period

may be assigned any value for h and T or a mode random to generate a realistic surface. Furthermore, h and T may either be made dependent on each other or statistically independent. In the case of the lunar crater, it is found that the rim height, rim base width, and crater depth are all almost linearly related to the crater diameter on the average, such as:

$$D/10 < h_1 < D/3 \qquad h_2 \simeq .1 h_1$$
$$d_1 \simeq .5D \qquad d_2 \simeq .55D. \qquad (2\text{-}6)$$

Thus, the crater diameter is the only random variable for the quasi-periodic surface component, such that given a crater diameter the quasi-periodic surface is completely specified.

The scalar Helmholtz integral is used to calculate the LM radar return power since ξ_R and ξ_P describe a complete set of statistics for this lunar module landing zone. Radar signal degradation is computed for each section along each of the landing approaches. This surface modeling is primarily limited by the resolution in interpreting the Orbiter and Surveyor lunar photographs.

The surface model generated by superposition of ξ_R and ξ_P is a posteriori stipulation based on the Surveyor and

Orbiter pictures; nevertheless, its statistical generality permits a very realistic surface representation and the prediction of radar return from it. Further research on the model is expected to yield more information on the scattering phenomena, such as secondary scattering and point-target diffraction.

CHAPTER III

RADAR RETURN FROM THE ONE-DIMENSIONAL NEW LUNAR SURFACE MODEL

A knowledge of radar doppler and velocity signal degradation is necessary for appropriate guidance and control of LM landing used in the Apollo program. A study of several possible landing sites shows that the distribution and size of craters and boulders are random, and the probability distribution of their sizes appears to be exponential in shape as shown in Fig. 3-1. A set of close-up pictures of the lunar surface taken by Russian Lunar 9 and American Surveyors and Orbiters I and II indicate that its local surface undulations are very rough in terms of the wavelength ($\lambda = 3$ cm) of the incident signal in the case of LM radars.

A surface roughness function denoting heights above and below the mean level can be described as t' a superposition of a number of rough surfaces such as

$$\xi = \xi_1 + \xi_2 + \xi_3 + \cdots \qquad (3\text{-}1)$$

The landing sites on the lunar surface may be modeled by such a superposition of a random roughness and a quasi-periodic surface in an interval T as a zero-th order model as shown in Fig. 2-1 and Fig. 2-3 where ξ_R is random gaussian component with zero mean and ξ_p is periodic with an exponential

Fig. 3-1. Crater Number Vs. Crater Diameter Curve

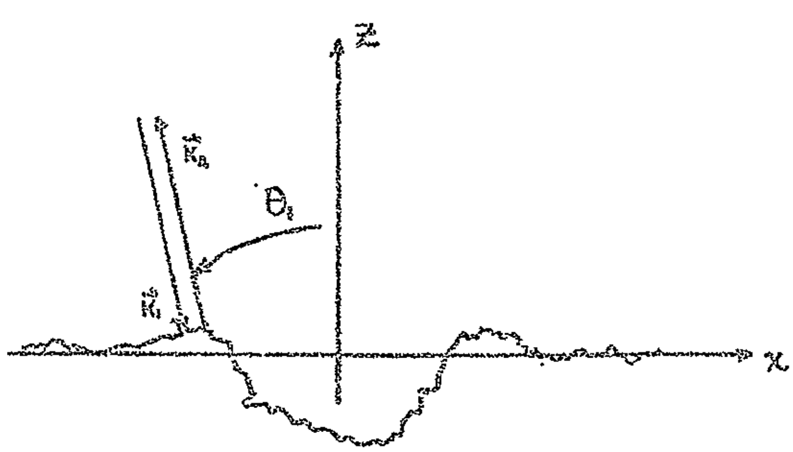

Fig. 3-2. Monostatic Radar Signal Return Geometry

probability density D of the crater diameter at the average elevation of the crater. The dimensions d_1, d_2, h_1, and h_2 are all functions of D, and T is fixed in order to maintain the identiyf of ξ_R and ξ_P; because if T was randomly varying ξ_P would tend to become ξ_R.

As a first order approximation, the surface is assumed invariant along the y-axis, and the radar return power can be calculated from this one-dimensional mode of the lunar surface. The general Kirchhoff integral is applied under the following assumptions:

a) The radar beam cross-section has dimensions large as compared to T.

b) The radius of curvature of the random rough surface is much greater than the wavelength of the incident radiation.

c) The incident radiation is a horizontally polarized plane wave.

d) Shadowing, multiple scattering and depolarization effect is neglected.

e) ξ_R and ξ_P are statistically independent.

$$E_2(\theta_1;\theta_2) = \frac{E_{20} F}{2L}\int_{-L}^{L} \exp(i\bar{V}\cdot\bar{r})\,dx \qquad (3\text{-}2)$$

where

$E_2(\theta_1;\theta_2)$ is the reflected field from the surface.

θ_1 and θ_2 are angles of incident and reflection as measured from the outward surface normal.

E_{20} is the field reflected in the direction of specular reflection ($\theta_2 = \theta_1$) by a smooth, perfectly conducting plane of the same dimensions under the same angle of incidence at the same distance.

$$F = \sec\theta_1 \frac{1 + \cos(\theta_1 + \theta_2)}{\cos\theta_1 + \cos\theta_2}$$

$4L^2$ is taken as a sampling area

$$\bar{v} = \bar{K}_1 - \bar{K}_2$$

$$v_x = k(\sin\theta_1 - \sin\theta_2)$$

$$v_z = -k(\cos\theta_1 + \cos\theta_2)$$

$$\bar{r} = X\bar{a}_x + (\xi_R + \xi_p)\bar{a}_z$$

ξ_R and ξ_p are functions of x denoting the height of the rough surface.

The scattering geometry is shown in Fig. 3-2 where $\theta_2 = -\theta_1$ and $F = 1/\cos^2\theta_1$.

The calculation of the monostatic scattered field with $L = nT$ from Eq. (3-2) is

$$E_s(\theta_1;\theta_2) = \frac{E_{20}F}{2nT}\sum_{\mu=-n}^{n-1}\int_{\mu T}^{(\mu+1)T}\exp[iV_x X + iV_z(\xi_R + \xi_p)]\,dx \quad (3\text{-}3)$$

$$E_s(\theta_1;\theta_2) = \frac{E_{20}F}{T}\frac{1}{2n}\sum_{\mu=-n}^{n-1}\exp(i2\pi\mu p)\int_{-\frac{T}{2}}^{\frac{T}{2}}\exp[iV_x x + iV_z(\xi_R + \xi_p)]\,dx \quad (3\text{-}4)$$

The generalized grating equation is

$$P = \frac{T}{\lambda}\left(\sin\theta_1 - \sin\theta_2\right)$$
$$= \frac{T V_x}{2\pi} \qquad (3\text{-}5)$$

where P is any real number satisfying the above grating equation for a given θ_1 and θ_2. The substitution of P in Eq. (3-4) yields:

$$E_s(\theta_1;\theta_2) = \frac{W E_{20} F}{T}\int_{-\frac{T}{2}}^{\frac{T}{2}} \exp\left[iV_x x + iV_z(\xi_R + \xi_P)\right] dx \qquad (3\text{-}6)$$

$$W = \frac{1}{2n}\sum_{m=-n}^{n-1} \exp(i 2\pi m p) \qquad (3\text{-}7)$$

The average return power is

$$\langle E_s E_s^* \rangle = \left\langle \frac{|W|^2 E_{20}^2 F^2}{T^2} \int_{-\frac{T}{2}}^{\frac{T}{2}}\int_{-\frac{T}{2}}^{\frac{T}{2}} \exp\left[iV_x(x_1 - x_2) + iV_z(\xi_{R_1} - \xi_{R_2}) + iV_z(\xi_{P_1} - \xi_{P_2})\right] dx_1 dx_2 \right\rangle \qquad (3\text{-}8)$$

where

$$\xi_{R_1} = \xi_R(x_1) \qquad \xi_{R_2} = \xi_R(x_2)$$
$$\xi_{P_1} = \xi_P(x_1) \qquad \xi_{P_2} = \xi_P(x_2) \qquad (3\text{-}9)$$

or

$$\langle E_s E_s^* \rangle = \left\langle \frac{|W|^2 E_{20}^2 F^2}{T^2} \int_{-\frac{T}{2}}^{\frac{T}{2}}\int_{-\frac{T}{2}}^{\frac{T}{2}} \exp\left[iV_x(x_1 - x_2) + iV_z(\xi_{P_1} - \xi_{P_2})\right] \left\langle \exp\left[iV_z(\xi_{R_1} - \xi_{R_2})\right]\right\rangle_{\xi_R} dx_1 dx_2 \right\rangle_{\xi_P} \qquad (3\text{-}10)$$

The average is taken over the statistically independent random variables ξ_R and ξ_P.

Now

$$\langle \exp[iV_2(\xi_{R_1} - \xi_{R_2})] \rangle_{\xi_R} = \int_{-\infty}^{\infty}\int_{-\infty}^{\infty} p(x_1; x_2)$$

$$\exp[iV_2(\xi_{R_1} - \xi_{R_2})]\, dx_1\, dx_2 \qquad (3\text{-}11)$$

where

$$p(x_1; x_2) = \frac{1}{2\pi\sigma^2\sqrt{1-C^2}} \exp -\left[\frac{x_1^2 - 2C x_1 x_2 + x_2^2}{2\sigma^2(1-C^2)}\right]. \qquad (3\text{-}12)$$

The characteristic function evaulated from Eq. (3-11) using Eq. (3-12) is (Middleton, 1960):

$$\langle \exp[iV_2(\xi_{R_1} - \xi_{R_2})] \rangle = \exp\left[-\sigma^2 V_2^2 \left(1 - \exp\frac{-|x_1 - x_2|}{B}\right)\right]$$

$$= \exp -(\sigma V_2)^2 \sum_{m=0}^{\infty} \frac{(\sigma V_2)^{2m}}{m!} \exp\left(\frac{-m|x_1 - x_2|}{B}\right) \qquad (3\text{-}13)$$

A transformation of x_1 and x_2 into x_2 and τ yields

$$x_1, x_2 \rightarrow x_2, \tau \qquad (3\text{-}14)$$

$$dx_1, dx_2 \rightarrow |J|\, dx_2\, d\tau \qquad (3\text{-}15)$$

$$|J| = 1 \qquad (3\text{-}16)$$

A substitute of the Jacobian in the average power Eq. (3-10) yields

$$\langle E_2 E_2^* \rangle = \Big\langle \frac{|W|^2 E_{20}^2 F^2}{T^2} \exp -(\sigma V_2)^2 \sum_{m=0}^{\infty} \frac{(\sigma V_2)^{2m}}{m!}$$

$$\int_{-\frac{T}{2}-x_2}^{\frac{T}{2}-x_2} \int_{-\frac{T}{2}}^{\frac{T}{2}} \exp\left(iV_x\tau - \frac{m|\tau|}{B}\right) \cdot \exp[iV_z(\xi_{P_1} - \xi_{P_2})]\, dx_2\, d\tau \Big\rangle_{\xi_P} \qquad (3\text{-}17)$$

The limits make it necessary to integrate over τ before integrating over X_2. However, by assuming that $B \ll \frac{T}{2}$ and that the integral of τ has value only at very small value of τ, it would not be erroneous to extend the limits to infinity instead of from $-\frac{T}{2}-X_2$ to $\frac{T}{2}-X_2$, since

$$\int_{-\frac{T}{2}-X_2}^{\frac{T}{2}-X_2} f(\tau)\,d\tau \doteq \int_{-\infty}^{\infty} f(\tau)\,d\tau \qquad (3\text{-}18)$$

Since the limits of integration on τ are approximated to be minus infinity to plus infinity, taking into account the divergent term representing the average return power as shown below:

$$\langle E_2 E_2^* \rangle = \langle E_2 \rangle \langle E_2^* \rangle + D\{E_2\} \qquad (3\text{-}19)$$

After simplifying, Eq. (3-2) becomes

$$E_2 = \frac{W E_{20} F}{T} \int_{-\frac{T}{2}}^{\frac{T}{2}} \exp\left[iV_x X + iV_2(\xi_2 + \xi_p)\right] dx \qquad (3\text{-}20)$$

the average of which is

$$\langle E_2 \rangle = \left\langle \frac{W E_{20} F}{T} \int_{-\frac{T}{2}}^{\frac{T}{2}} \exp(iV_x X + iV_2 \xi_p) \langle \exp(iV_2 \xi_2) \rangle dx \right\rangle \qquad (3\text{-}21)$$

The characteristic function is calculated to be (Middleton, 1960)

$$\langle \exp(iV_2 \xi_2) \rangle = \exp -\tfrac{1}{2}(\sigma V_2)^2 \qquad (3\text{-}22)$$

and

$$\langle E_z \rangle = \left\langle \frac{W E_{zo} F}{T} \exp -\tfrac{1}{2}(\sigma V_z)^2 \int_{-\frac{T}{2}}^{\frac{T}{2}} \exp(iV_x x + iV_z \xi_p)\, dx \right\rangle_{\xi_p} \quad (3\text{-}23)$$

Let

$$I = \int_{-\frac{T}{2}}^{\frac{T}{2}} \exp(iV_x x + iV_z \xi_p)\, dx$$

$$= I_1 + I_2 + I_3 \quad (3\text{-}24)$$

with

$$I_1 = \int_{-\frac{T}{2}}^{-d_2} \exp(iV_x x)\, dx + \int_{d_2}^{\frac{T}{2}} \exp(iV_x x)\, dx$$

$$= \frac{\sin V_x \frac{T}{2} - \sin V_x d_2}{V_x/2} \quad (3\text{-}25)$$

$$I_2 = \int_{-d_2}^{-d_1} \exp\left[iV_x x + iV_z h_2 \sin\frac{\pi(-x-d_1)}{d_2-d_1}\right] dx + \int_{d_1}^{d_2} \exp\left[iV_x x + iV_z h_2 \sin\frac{\pi(x-d_1)}{d_2-d_1}\right] dx$$

$$= \sum_{p=-\infty}^{\infty} J_p(V_z h_2)\left[\frac{e^{-iV_x d_1}\cdot e^{ip\pi} - e^{-iV_x d_2} + e^{iV_x d_2}\cdot e^{ip\pi} - e^{iV_x d_1}}{i(V_x + \frac{p\pi}{d_2-d_1})}\right] \quad (3\text{-}26)$$

$$I_3 = \int_{-d_1}^{d_1} \exp\left[iV_x x - iV_z h_1 \cos\frac{\pi x}{2d_1}\right] dx$$

$$= \sum_{f=-\infty}^{\infty} i^f\, J_f(-V_z h_1)\, \frac{\sin(V_x + \frac{f\pi}{2d_1})d_1}{(V_x + \frac{f\pi}{2d_1})/2} \quad (3\text{-}27)$$

Substituting Eq. (3-25), (3-26), and (3-27) into Eq. (3-23), one obtains

$$\langle E_z \rangle = \Bigg\langle \frac{W E_{zo} F}{T} \exp -\tfrac{1}{2}(\sigma V_z)^2 \Bigg\{ \frac{\sin V_x \frac{T}{2} - \sin V_x d_2}{V_x/2}$$

$$+ \sum_{p=-\infty}^{\infty} J_p(V_z h_2)\left[\frac{e^{iV_x d_1}\cdot e^{ip\pi} - e^{-iV_x d_2} + e^{iV_x d_2}\cdot e^{ip\pi} - e^{iV_x d_1}}{i(V_x + \frac{p\pi}{d_2-d_1})}\right]$$

$$+\sum_{f=-\infty}^{\infty} i^{f}\, J_f(-V_z h_1)\, \frac{\sin(V_x + \frac{f\pi}{2d_1})d_1}{(V_x + \frac{f\pi}{2d_1})/2} \Bigg\} \Bigg\rangle_{\xi_p} \qquad (3\text{-}28)$$

Taking the conjugate of Eq. (3-28), one obtains

$$\langle E_2^* \rangle = \Bigg\langle \frac{W E_{20} F}{T} \exp -\tfrac{1}{2}(\sigma V_z)^2 \Bigg\{ \frac{\sin V_x \frac{T}{2} - \sin V_x d_2}{V_x/2}$$

$$+ \sum_{p=-\infty}^{\infty} J_p(V_z h_2) \left[\frac{-e^{iV_x d_1} \cdot e^{ip\pi} + e^{iV_x d_2} - e^{-iV_x d_2} \cdot e^{ip\pi} + e^{-iV_x d_1}}{i(V_x + \frac{p\pi}{d_2 - d_1})} \right]$$

$$+ \sum_{f=-\infty}^{\infty} i^{f} J_f(+V_z h_1) \frac{\sin(V_x - \frac{f\pi}{2d_1})d_1}{(V_x - \frac{f\pi}{2d_1})/2} \Bigg\} \Bigg\rangle_{\xi_p} \qquad (3\text{-}29)$$

The second term in Eq. (3-19) is now calculated to be as

$$D\{E_2\} = \Bigg\langle K_1 \int_{-\infty}^{\infty} \exp\left[iV_x\tau - \frac{m|\tau|}{B}\right]$$

$$\int_{-\frac{T}{2}}^{\frac{T}{2}} \exp\left[iV_z(\xi_{p_1} - \xi_{p_2})\right] dx_2\, d\tau \Bigg\rangle_{\xi_p} \qquad (3\text{-}30)$$

with

$$K_1 = \frac{|W|^2 E_{20}^2 F^2}{T^2} \exp -(\sigma V_z)^2 \sum_{m=1}^{\infty} \frac{(\sigma V_z)^{2m}}{m!} \qquad (3\text{-}31)$$

Since ξ_{p_1} and ξ_{p_2} are the only functions in the integrand containing x_2, it may be evaluated separately.

Let

$$I = \int_{-\frac{T}{2}}^{\frac{T}{2}} \exp\left[iV_z(\xi_{p_1} - \xi_{p_2})\right] dx_2$$

$$= I_1 + I_2 + I_3 \quad \text{(See Fig. 2-3)} \qquad (3\text{-}32)$$

$$I_1 = \int_{-\frac{T}{2}}^{-d_2} dx_2 + \int_{d_2}^{\frac{T}{2}} dx_2 \qquad (3\text{-}33)$$

$$I_2 = \int_{-d_2}^{-d_1} \exp\left[iV_2h_2\left\{\sin\frac{\pi(-\tau-x_2-d_1)}{d_2-d_1} - \sin\frac{\pi(-x_2-d_1)}{d_2-d_1}\right\}\right] dx_2$$

$$+ \int_{d_1}^{d_2} \exp\left[iV_2h_2\left\{\sin\frac{\pi(\tau+x_2-d_1)}{d_2-d_1} - \sin\frac{\pi(x_2-d_1)}{d_2-d_1}\right\}\right] dx_2 \qquad (3\text{-}34)$$

$$I_3 = \int_{-d_1}^{d_1} \exp\left[-iV_2h_1\left\{\cos\frac{\pi(\tau+x_2)}{2d_1} - \cos\frac{\pi x_2}{2d_1}\right\}\right] dx_2 \qquad (3\text{-}35)$$

Further integration yields:

$$I_1 = \tau - 2d_2 \qquad (3\text{-}36)$$

$$I_2 = 2(d_2-d_1)\sum_{p=-\infty}^{\infty}\sum_{q=-\infty}^{\infty}(i)^{p+q} J_p(V_2h_2)\, J_q(-V_2h_2)$$

$$\left[\frac{\sin\frac{\pi}{2}(p+q)}{\frac{\pi}{2}(p+q)}\right]\cos\frac{p\pi\tau}{d_2-d_1}, \text{ AND} \qquad (3\text{-}37)$$

$$I_3 = 2d_1\sum_{f=-\infty}^{\infty}\sum_{g=-\infty}^{\infty}(i)^{f+g} J_f(-V_2h_1)\, J_g(V_2h_1)$$

$$\left[\frac{\sin\frac{\pi}{2}(f+g)}{\frac{\pi}{2}(f+g)}\right]\exp\left(\frac{if\pi\tau}{2d_1}\right). \qquad (3\text{-}38)$$

$$D\{E_2\} = \left\langle K_1\int_{-\infty}^{\infty}\exp\left[iV_2\tau - \frac{m l \pi}{B}\right](I_1+I_2+I_3)\,d\tau\right\rangle_{\xi_p}$$

$$= \left\langle K_1(I_1' + I_2' + I_3')\right\rangle_{\xi_p} \qquad (3\text{-}39)$$

WITH

$$I_1' = \int_{-\infty}^{\infty} \exp(iV_x\tau) \cdot \exp\left(-\frac{m|\tau|}{B}\right)(T - 2d_2)\, d\tau$$

$$= 2(T - 2d_2) \int_0^{\infty} \exp\left(-\frac{m\tau}{B}\right) \cos V_x\tau \, d\tau$$

$$= 2(T - 2d_2) \frac{m/B}{\left(\frac{m}{B}\right)^2 + V_x^2} \qquad (3-40)$$

$$I_2' = 2(d_2 - d_1) \sum_{p=-\infty}^{\infty} \sum_{q=-\infty}^{\infty} (i)^{p+q} J_p(V_z h_1)\, J_q(-V_z h_2)$$

$$\left[\frac{\sin \frac{\pi}{2}(p+q)}{\frac{\pi}{2}(p+q)}\right] \int_{-\infty}^{\infty} \exp(iV_x\tau) \cdot \exp\left(-\frac{m|\tau|}{B}\right) \cos \frac{p\pi\tau}{d_2 - d_1}\, d\tau$$

$$= 2(d_2 - d_1) \sum_{p=-\infty}^{\infty} \sum_{q=-\infty}^{\infty} (i)^{p+q} J_p(V_z h_1)\, J_q(-V_z h_2)$$

$$\left[\frac{\sin \frac{\pi}{2}(p+q)}{\frac{\pi}{2}(p+q)}\right] \left[\frac{\frac{m}{B}}{\left(\frac{m}{B}\right)^2 + \left(V_x + \frac{p\pi}{d_2 - d_1}\right)^2} +\right.$$

$$\left. + \frac{\frac{m}{B}}{\left(\frac{m}{B}\right)^2 + \left(V_x - \frac{p\pi}{d_2 - d_1}\right)^2}\right], \text{ AND} \qquad (3-41)$$

$$I_3' = 4 d_1 \sum_{f=-\infty}^{\infty} \sum_{g=-\infty}^{\infty} (i)^{f+g} J_f(-V_z h_1)\, J_g(V_z h_1)$$

$$\left[\frac{\sin \frac{\pi}{2}(f+g)}{\frac{\pi}{2}(f+g)}\right] \int_0^{\infty} \exp\left(-\frac{m\tau}{B}\right) \cos\left(V_x + \frac{f\pi}{2d_1}\right)\tau\, d\tau$$

$$= 4 d_1 \sum_{f=-\infty}^{\infty} \sum_{g=-\infty}^{\infty} (i)^{f+g} J_f(-V_z h_1) J_g(V_z h_1)$$

$$\left[\frac{\sin \frac{\pi}{2}(f+g)}{\frac{\pi}{2}(f+g)}\right] \left[\frac{\frac{m}{B}}{\left(\frac{m}{B}\right)^2 + \left(V_x + \frac{f\pi}{2d_1}\right)^2}\right] \quad (3\text{-}42)$$

The variance of the return signal is,

$$D\{E_2\} = \Big\langle K_1 \Big\{ 2(T - 2d_2) \frac{\frac{m}{B}}{\left(\frac{m}{B}\right)^2 + V_x^2}$$

$$+ 2(d_2 - d_1) \sum_{p=-\infty}^{\infty} \sum_{q=-\infty}^{\infty} (i)^{p+q} J_p(V_z h_2) J_q(-V_z h_2)$$

$$\left[\frac{\sin \frac{\pi}{2}(p+q)}{\frac{\pi}{2}(p+q)}\right] \left[\frac{\frac{m}{B}}{\left(\frac{m}{B}\right)^2 + \left(V_x + \frac{p\pi}{d_2 - d_1}\right)^2} + \frac{\frac{m}{B}}{\left(\frac{m}{B}\right)^2 + \left(V_x - \frac{p\pi}{d_2 - d_1}\right)^2}\right]$$

$$+ 4 d_1 \sum_{f=-\infty}^{\infty} \sum_{g=-\infty}^{\infty} (i)^{f+g} J_f(-V_z h_1) J_g(V_z h_1)$$

$$\left[\frac{\sin \frac{\pi}{2}(f+g)}{\frac{\pi}{2}(f+g)}\right] \left[\frac{\frac{m}{B}}{\left(\frac{m}{B}\right)^2 + \left(V_x + \frac{f\pi}{2d_1}\right)^2}\right] \Big\} \Big\rangle_{\xi_p} \quad (3\text{-}43)$$

The complete solution for the averaged radar return is the DC term, which is the product of Eq. (3-28) and (3-29), plus the variance of Eq. (3-43).

In the absence of craters or hills, i. e., $\xi_p = 0$

$$\langle E_2 \rangle \langle E_2^* \rangle = |W|^2 E_{20}^2 F^2 \exp -(\sigma V_z)^2 \left[\frac{\sin V_x T/2}{V_x T/2}\right]^2 \quad (3\text{-}44)$$

and $$D\{E_2\} = |W|^2 E_{20}^2 F^2 \cdot (\sigma V_z)^2 \sum_{m=1}^{\infty} \frac{(\sigma V_z)^{2m} \; 2\frac{m}{B}}{m! \cdot T\left[\left(\frac{m}{B}\right)^2 + V_x^2\right]} \quad (3\text{-}45)$$

Therefore,

$$\langle E_2 E_2^* \rangle \Big|_{\xi_p = 0} = |W|^2 E_{20}^2 F^2 \exp -(\sigma V_z)^2 \Big[\frac{\sin V_x \frac{T}{2}}{V_x \frac{T}{2}} + \sum_{m=1}^{\infty} \frac{(\sigma V_z)^{2m}}{m!} \frac{2\frac{m}{B}}{T[(\frac{m}{B})^2 + V_x^2]} \Big] \qquad (3\text{-}46)$$

The factor $|W|^2$ for the pure random surface equals unity and the result checks well with that calculated by Hayre and Kaufman (1965).

In the absence of the general roughness, $\xi_R = 0$

$$\sigma = 0 \qquad (3\text{-}47)$$

$$\frac{1}{B} = 0 \qquad (3\text{-}48)$$

and Eq. (3-19) becomes

$$\langle E_2 E_2^* \rangle \Big|_{\xi_R = 0} = \frac{|W|^2 E_{20}^2 F^2}{T^2} \Big\langle \Big\{ \frac{\sin V_x \frac{T}{2} - \sin V_x d_2}{V_x/2}$$

$$+ \sum_{p=-\infty}^{\infty} J_p(V_z h_2) \Big[\frac{e^{-iV_x d_1} \cdot e^{ip\pi} - e^{-iV_x d_2} + e^{iV_x d_2} \cdot e^{ip\pi} - e^{iV_x d_1}}{i(V_x + \frac{p\pi}{d_2 - d_1})} \Big]$$

$$+ \sum_{f=-\infty}^{\infty} i^f J_f(-V_z h_1) \frac{\sin(V_x + \frac{f\pi}{2d_1}) d_1}{(V_x + \frac{f\pi}{2d_1})/2} \Big\} \Big\rangle_{\xi_p} \times$$

$$\Big\langle \Big\{ \frac{\sin V_x \frac{T}{2} - \sin V_x d_2}{V_x/2}$$

$$+ \sum_{p=-\infty}^{\infty} J_p(V_z h_2) \Big[\frac{-e^{iV_x d_1} \cdot e^{ip\pi} + e^{iV_x d_2} - e^{-iV_x d_2} \cdot e^{ip\pi} + e^{-iV_x d_1}}{i(V_x + \frac{p\pi}{d_2 - d_1})} \Big].$$

$$+ \sum_{f=-\infty}^{\infty} i^f J_f(V_z h_1) \frac{\sin(V_x - \frac{f\pi}{2d_1}) d_1}{(V_x - \frac{f\pi}{2d_1})/2} \Big\} \Big\rangle_{\xi_p} \qquad (3\text{-}49)$$

In the absence of both ξ_x and ξ_p, the surface becomes a mirror reflector, and its radar reflectivity is

$$\langle E_z E_z^* \rangle \Big|_{\substack{\xi_x=0 \\ \xi_p=0}} = E_{20}^2 F^2 \left[\frac{\sin V_x \frac{T}{2}}{V_x \frac{T}{2}} \right]^2 \qquad (3\text{-}50)$$

For the monostatic case, one has

$$F^2 = \frac{1}{\cos^4 \theta_1} \qquad (3\text{-}51)$$

$$V_x = \frac{4\pi}{\lambda} \sin \theta_1 \qquad (3\text{-}52)$$

The curves of F^2 vs. θ_1 and $\left[\frac{\sin V_x \frac{T}{2}}{V_x \frac{T}{2}} \right]^2$ vs. θ_1 are presented in Fig. 3-3. If T is $\gg \lambda$, $\left[\frac{\sin V_x \frac{T}{2}}{V_x \frac{T}{2}} \right]^2$ decays very rapidly, and the product of the two curves may be approximated by an impulse, or

$$\langle E_z E_z^* \rangle \Big|_{\substack{\xi_x=0 \\ \xi_p=0}} = E_{20}^2 \, \delta(\theta_1) \qquad (3\text{-}53)$$

The significant terms in the Eq. (3-19) for the conditions $\sigma V_z \ll 1$, $\sigma V_z \simeq 1$ and $\sigma V_z \gg 1$ which correspond to slight, moderate and very rough surfaces, respectively, have been discussed in great detail by Beckman (1963). In the case of the lunar surface where the general random surface appears to be very rough in terms of 3 cm wavelength (as shown in Surveyor pictures) σV_z is indeed large compared to 1, Eq. (3-19) becomes

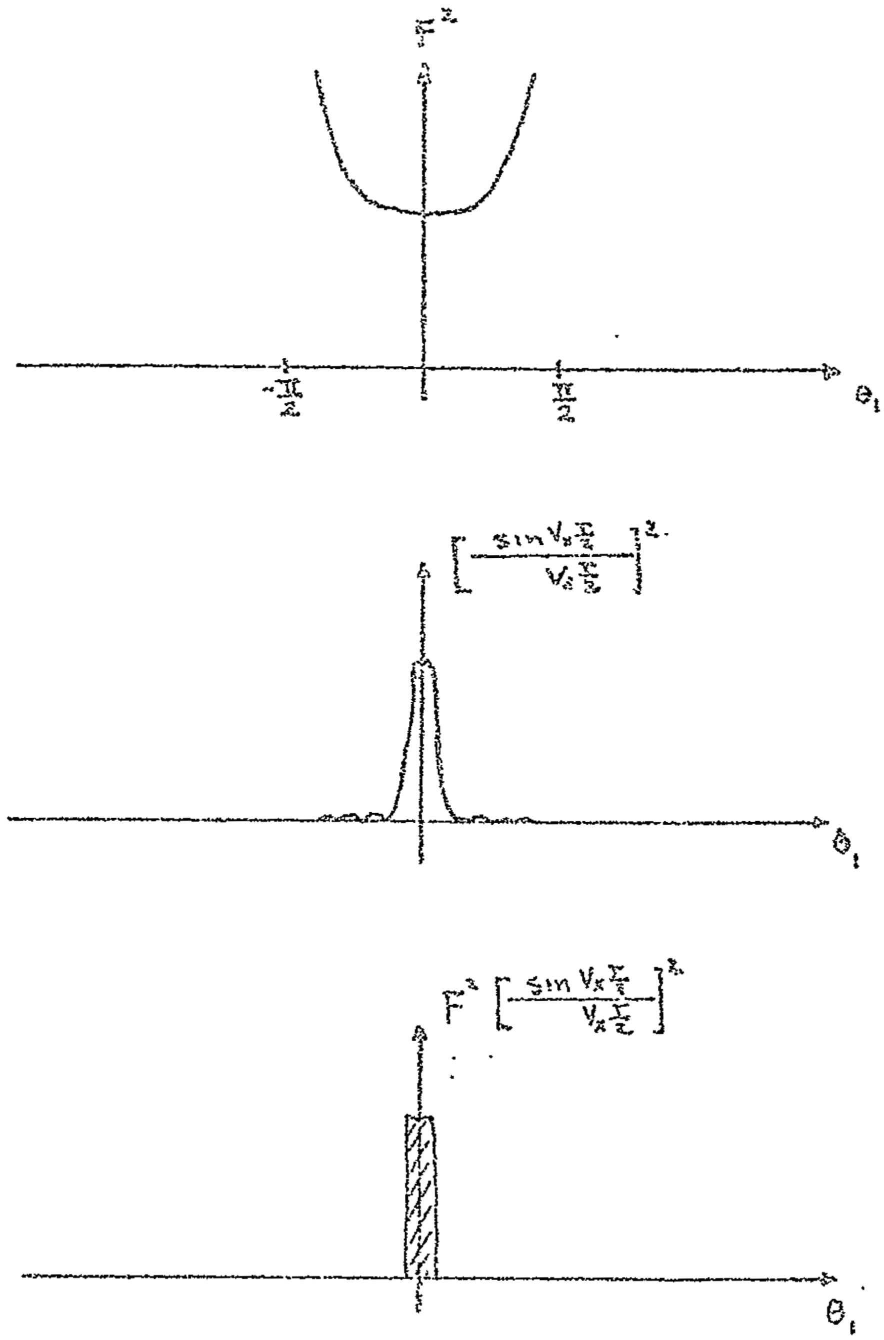

Fig. 3-3. The Impulse Approximation for the Monostatic Mirror Reflector

$$\langle E_2 E_2^* \rangle \simeq D\left\{ E_2 \right\} \tag{3-54}$$

and

$$\exp -(\sigma V_z)^2 \left(1 - e^{-\frac{|\tau|}{B}}\right) \simeq \exp -(\sigma V_z)^2 \frac{|\tau|}{B} \tag{3-55}$$

Substituting Eq. (3-55) in (3-30) for the calculation of $\langle E_2 E_2^* \rangle$, the resulting expression is

$$\begin{aligned} \langle E_2 E_2^* \rangle = \Big\langle \frac{|W|^2 E_{20}^2 F^2}{T^2} \Big\{ & 2(T - 2d_2) \frac{(\sigma V_z)^2 B}{(\sigma V_z)^4 + V_x^2 B^2} \\ & + 2(d_2 - d_1) \sum_{p=-\infty}^{\infty} J_p^2 (V_z h_2) \Big[\frac{(\sigma V_z)^2 B}{(\sigma V_z)^4 + \left(V_x + \frac{p\pi}{d_2 - d_1}\right)^2 B^2} \\ & + \frac{(\sigma V_z)^2 B}{(\sigma V_z)^4 + \left(V_x - \frac{p\pi}{d_2 - d_1}\right)^2 B^2} \Big] + 4 d_1 \sum_{f=-\infty}^{\infty} J_f^2 (V_z h_1) \\ & \Big[\frac{(\sigma V_z)^2 B}{(\sigma V_z)^4 + \left(V_x + \frac{2\pi f}{2 d_1}\right)^2 B^2} \Big] \Big\} \Big\rangle_{\mathfrak{F}_p} \end{aligned} \tag{3-56}$$

In Fig. 3-4, a curve is plotted using Eq. (3-56) with the following parameters:

λ = 3 cm

σ = .3 cm

B = 3 cm

$|W|^2$ = 1

T = 30 meters

$P_{\mathfrak{F}_p}(D)$ = .05 exp (−.05D)

d_1 = .5D

d_2 = .55D

h_1 = .2D

h_2 = .02D

The results of other models (Hayre, 1962; Muhleman, 1964) and experimental results (Evans and Pettingel, 1963) dealing with lunar radar return are also plotted in Fig. 3-4, and a comparison of these with results obtained by the model used in this work shows very good comparison.

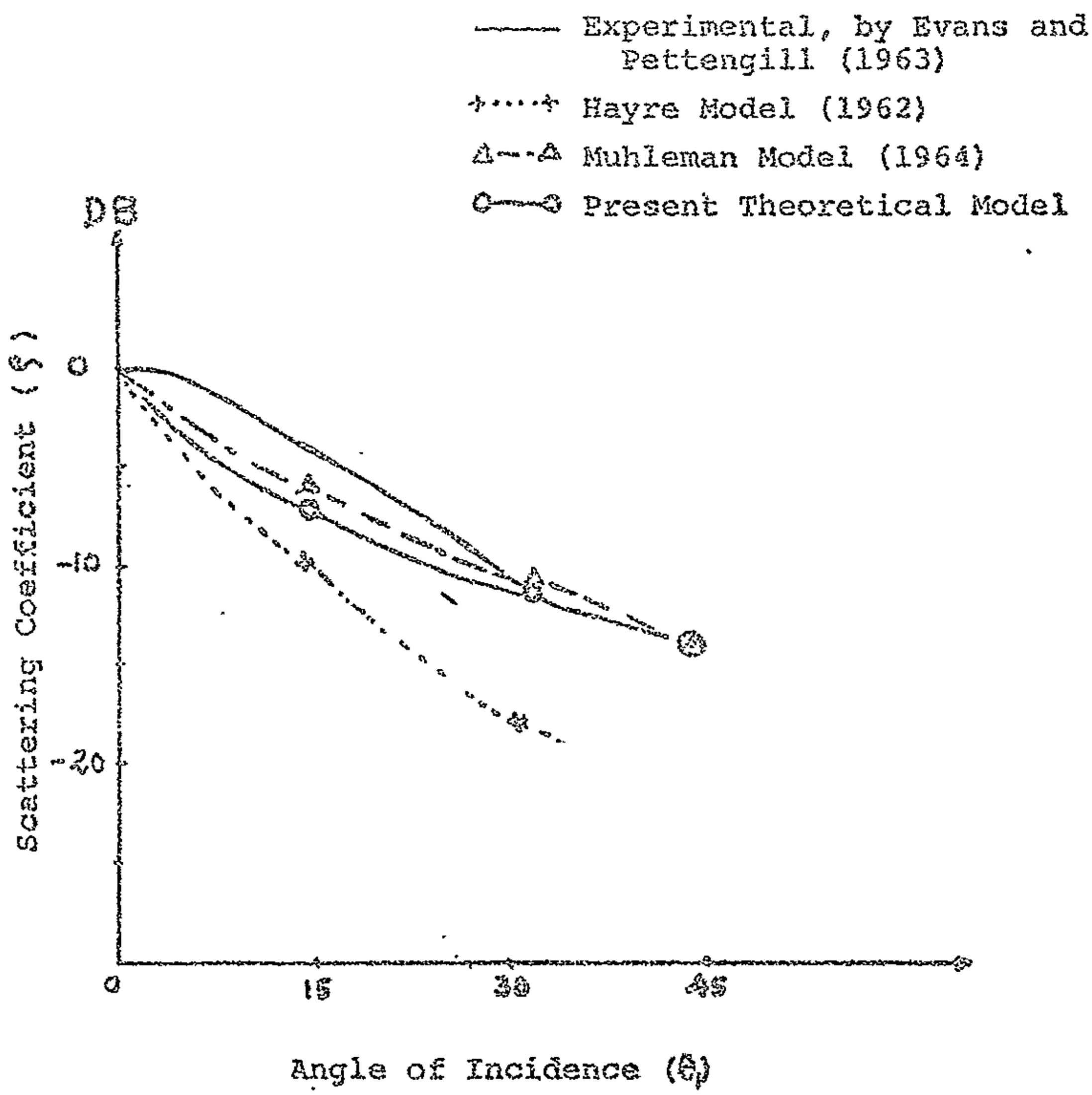

$$\rho = \frac{\langle E_1 E_s^* \rangle}{|E_{2o}^2|}$$

Fig. 3-4. Scattering Coefficient Vs. the Angle of Incidence

CHAPTER IV

RADAR RETURN FROM THE TWO-DIMENSIONAL NEW LUNAR SURFACE MODEL

The calculations of average radar return power in the last chapter were made for one-dimensional lunar surface model in order to simplify the mathematical procedure. The two-dimensional case is presented in this chapter.

The data on the LM trajectory shows that the altimeter beam has an incident angle (θ_1) variation from zero to forty degrees with respect to the outward average lunar surface normal. Since the radar system is a monostatic case, the reflection angle (θ_2) is the negative of the incident angle (θ_1) and the lateral deviation angle (θ_3) is zero. (See Fig. 3-2.) The close-up pictures taken by Surveyor II indicate that the general surface is very rough in terms of the incident wavelength (3 cm). The surface function is taken as a composite of a random and a periodic roughness. (See Figs. 2-1, 2-2 and 2-3.)

The assumptions similar to those made for one-dimensional case are made here as well.

The return field E_2 for a two-dimensional surface is given by (Beckman, et al, 1963):

$$E_2 = \frac{E_{20}F}{A} \int_{-L_x}^{L_x}\int_{-L_y}^{L_y} \exp(i\bar{V}\cdot\bar{r})\ dx\ dy$$

$$= \frac{W_x W_y E_{20} F}{T^2} \int_{-\frac{T}{2}}^{\frac{T}{2}} \int_{-\frac{T}{2}}^{\frac{T}{2}} \exp\left[iV_x x + iV_y y + iV_z (\xi_R + \xi) \right] dx\, dy \tag{4-1}$$

where

$$W_x = \frac{\sin(2np\pi)}{2n \sin(p\pi)} \exp(-ip\pi) \tag{4-2}$$

$$W_y = \frac{\sin(2mq\pi)}{2m \sin(q\pi)} \exp(-iq\pi) \tag{4-3}$$

$$n = \frac{L_x}{T}, \quad m = \frac{L_y}{T} \tag{4-4}$$

$$p = \frac{T V_x}{2\pi}, \quad q = \frac{T V_y}{2\pi} \tag{4-5}$$

E_{20} is the normal specular return from a smooth surface

$$F = \frac{1 + \cos\theta_1 \cos\theta_2 - \sin\theta_1 \sin\theta_2 \cos\theta_3}{\cos\theta_1 (\cos\theta_1 + \cos\theta_2)} \tag{4-6}$$

$$V_x = \frac{2\pi}{\lambda} (\sin\theta_1 - \sin\theta_2), \quad V_y = \frac{-2\pi}{\lambda} \sin\theta_2 \sin\theta_3 \tag{4-7}$$

$$V_z = \frac{-2\pi}{\lambda} (\cos\theta_1 + \cos\theta_2) \tag{4-8}$$

The average power is therefore given by

$$\langle E_2 E_2^* \rangle = \left\langle \frac{|W_x|^2 |W_y|^2 E_{20}^2 F^2}{T^4} \int_{-\frac{T}{2}}^{\frac{T}{2}} \int_{-\frac{T}{2}}^{\frac{T}{2}} \int_{-\frac{T}{2}}^{\frac{T}{2}} \int_{-\frac{T}{2}}^{\frac{T}{2}} \exp\left[iV_x (x_1 - x_2) \right.\right.$$

$$\left. + iV_y (y_1 - y_2) + iV_z (\xi_{p_1} - \xi_{p_2}) \right] \cdot$$

$$\left\langle \exp\left[iV_z (\xi_{R_1} - \xi_{R_2}) \right] \right\rangle_{\xi_R} dx_1\, dx_2\, dy_1\, dy_2 \Big\rangle_{\xi_p} \tag{4-9}$$

$$\xi_{R_1} = \xi_R(x_1, y_1), \qquad \xi_{R_2} = \xi_R(x_2, y_2)$$

$$\xi_{P_1} = \xi_P(x_1, y_1), \qquad \xi_{P_2} = \xi_P(x_2, y_2) \qquad (4\text{-}10)$$

Since the roughness is isotropic, its correlation between two points on the $Z = 0$ plane is a function of only the magnitude of the distance between the two points $P_1(x_1, y_1)$ and $P_2(x_2, y_2)$. Let the distance between the two points P_1 and P_2 be τ, where

$$\tau = \sqrt{(x_1 - x_2)^2 + (y_1 - y_2)^2} \qquad (4\text{-}11)$$

Then $\langle \exp[iV_z(\xi_{R_1} - \xi_{R_2})] \rangle$ can be treated as a one-dimensional second order random process, and the characteristic function in terms of τ is found as

$$\Phi(\tau) = \exp -(\sigma V_z)^2 \sum_{m=0}^{\infty} \frac{(\sigma V_z)^{2m}}{m!} \exp\left(-\frac{m\tau^2}{B}\right). \qquad (4\text{-}12)$$

A set of new variables may be defined as follows:

$$x_1 - x_2 = \tau \cos\phi \qquad (4\text{-}13)$$

$$y_1 - y_2 = \tau \sin\phi \qquad (4\text{-}14)$$

$$\phi = \operatorname{Tan}^{-1} \frac{y_1 - y_2}{x_1 - x_2} \qquad (4\text{-}15)$$

Now, transforming x_1, x_2, y_1, y_2 into x_1, y_1, τ, ϕ where $x_1 = x_1$

$$x_2 = x_1 - \tau \cos\phi$$

$$y_1 = y_1 \qquad (4\text{-}16)$$

$$y_2 = y_1 - \tau \sin\phi$$

one obtains

$$dx_1\ dx_2\ dy_1\ dy_2 = |J| \quad dx_1\ dy_1\ d\tau \quad d\phi \tag{4-17}$$

where

$$|J| = \begin{vmatrix} \frac{\partial x_1}{\partial x_1} & \frac{\partial x_1}{\partial y_1} & \frac{\partial x_1}{\partial \tau} & \frac{\partial x_1}{\partial \phi} \\ \frac{\partial x_2}{\partial x_1} & \frac{\partial x_2}{\partial y_1} & \frac{\partial x_2}{\partial \tau} & \frac{\partial x_2}{\partial \phi} \\ \frac{\partial y_1}{\partial x_1} & \frac{\partial y_1}{\partial y_1} & \frac{\partial y_1}{\partial \tau} & \frac{\partial y_1}{\partial \phi} \\ \frac{\partial y_2}{\partial x_1} & \frac{\partial y_2}{\partial y_1} & \frac{\partial y_2}{\partial \tau} & \frac{\partial y_2}{\partial \phi} \end{vmatrix}$$

$$= \begin{vmatrix} 1 & 0 & 0 & 0 \\ 1 & 0 & -\cos\phi & \tau \sin\phi \\ 0 & 1 & 0 & 0 \\ 0 & 1 & -\sin\phi & -\tau\cos\phi \end{vmatrix}$$

$$= \tau \cos^2\phi + \tau \sin^2\phi = \tau \tag{4-18}$$

This transformation process introduces the corresponding change of variables and limits as

$$\xi_{p_1} = \xi_p\,(x_1\,,\,y_1) \tag{4-19}$$

$$\xi_{p_2} = \xi_p\,(x_1 - \tau\cos\phi\,,\ y_1 - \tau \sin\phi) \tag{4-20}$$

$$-\frac{T}{2} < x_1 < \frac{T}{2} \tag{4-21}$$

$$-\frac{T}{2} < y_1 < \frac{T}{2} \tag{4-22}$$

$$\sqrt{(x_1 - \tfrac{T}{2})^2 + (y_1 - \tfrac{T}{2})^2} < \tau < \sqrt{(x_1 + \tfrac{T}{2})^2 + (y_1 + \tfrac{T}{2})^2} \tag{4-23}$$

$$\mathrm{TAN}^{-1}\left(\frac{y_1 - \frac{T}{2}}{x - \frac{T}{2}}\right) < \phi < \mathrm{TAN}^{-1}\left(\frac{y_1 + \frac{T}{2}}{x_1 + \frac{T}{2}}\right) \tag{4-24}$$

The limits of τ and ϕ are functions of x_1 and y_1 which vary from $-\frac{T}{2}$ to $\frac{T}{2}$ in each interval.

It is assumed that the autocorrelation C of ξ_R is insignificantly small for τ greater than T/2; and that the term $\exp(\frac{-|\tau|}{B})$ converges very rapidly. Therefore, the integral has major contribution for small τ, and it is possible to extend the limits on τ from zero to infinity.

The limits on the angle ϕ are integrated from $\phi_1 = \tan^{-1}\left(\frac{y_1+\frac{T}{2}}{x_1+\frac{T}{2}}\right)$ to $\phi_2 = \tan^{-1}\left(\frac{y_1-\frac{T}{2}}{x_1-\frac{T}{2}}\right)$ where x_1 and y_1 take on values between $-T/2$ and $T/2$ respectively. However, for all values of x_1 and y_1, ϕ is always bounded between zero and 2π.

And the transformed integral becomes

$$\langle E_2 E_2^* \rangle = \Big\langle \frac{|w_x|^2 |w_y|^2 E_{20}^2 F^2}{T^4} \int_{-\frac{T}{2}}^{\frac{T}{2}} \int_{-\frac{T}{2}}^{\frac{T}{2}} \int_0^{2\pi} \int_0^{\infty} \exp\Big[iV_x \tau \cos\phi + iV_y \tau \sin\phi + iV_z(\xi_1 - \xi_2)\Big] \Phi(\tau)\, \tau\, d\tau\, d\phi\, dx_1\, dy_1 \Big\rangle_{\xi_p} \quad (4\text{-}25)$$

In order to avoid a divergent integral, it is necessary to rearrange Eq. (4-25) by noting that

$$\langle E_2 E_2^* \rangle = \langle E_2 \rangle \langle E_2^* \rangle + D\{E_2\} \quad (4\text{-}26)$$

where

$$\langle E_2 \rangle = \Big\langle \frac{w_x w_y E_{20} F}{T^2} \int_{-\frac{T}{2}}^{\frac{T}{2}} \int_{-\frac{T}{2}}^{\frac{T}{2}} \exp[iV_x x + iV_y y + iV_z \xi_p] \langle \exp(iV_z \xi_R) \rangle\, dx\, dy \Big\rangle_{\xi_p}$$

$$= \Big\langle \frac{w_x w_y E_{20} F}{T^2} \exp -\tfrac{1}{2}(\sigma V_z)^2 \int_{-\frac{T}{2}}^{\frac{T}{2}} \int_{-\frac{T}{2}}^{\frac{T}{2}} \exp[iV_x x + iV_y y + iV_z \xi_p]\, dx\, dy \Big\rangle_{\xi_p} \quad (4\text{-}27)$$

After performing the polar transformation

$$\langle E_2 \rangle \doteq \left\langle \frac{W_x W_y E_{20} F}{T^2} \exp -\tfrac{1}{2}(\sigma V_z)^2 \cdot \left[I_1 + I_2 + I_3 \right] \right\rangle_{\xi, \rho} \quad (4\text{-}28)$$

(see Fig. 2-2) with

$$I_1 = T^2 - \pi d_2^2 \quad (4\text{-}29)$$

$$I_2 = \int_0^{2\pi}\int_{d_1}^{d_2} \exp\left[iV_x r\cos\theta + iV_y r\sin\theta + iV_z h_2 \sin\frac{\pi(r-d_1)}{d_2-d_1}\right] r\,dr\,d\theta$$

$$= 4\pi \sum_{p=1}^{\infty}\sum_{s=0}^{\infty} J_{-p}(V_z h_2)\frac{(-1)^s}{s!\,s!}\frac{(V_x^2+V_y^2)^s}{4^s}\cdot$$

$$\exp\left(\frac{-i2\pi p d_1}{d_2-d_1}\right)\left[\frac{d_2^{2s+2}-d_1^{2s+2}}{4s+4} - \sum_{a=0}^{2s+1}\frac{(2s+1)!}{a!}\cdot\right.$$

$$\left.\left(\frac{d_2-d_1}{-i2\pi p}\right)^{2s+2-a}\left(e^{\frac{i2\pi p d_2}{d_2-d_1}} d_2^a - e^{\frac{i2\pi p d_1}{d_2-d_1}} d_1^a\right)\right]. \quad (4\text{-}30)$$

$$I_3 = \int_0^{2\pi}\int_0^{d_1} \exp\left[iV_x r\cos\theta + iV_y r\sin\theta - iV_z h_1 \cos\frac{\pi r}{2d_1}\right] r\,dr\,d\theta$$

$$= 4\pi \sum_{f=1}^{\infty}\sum_{s=0}^{\infty} i^f J_f(-V_z h_1)\frac{(-1)^s}{s!\,s!}\cdot\frac{(V_x^2+V_y^2)^s}{4^s}\cdot$$

$$\left[\frac{d_1^{2s+2}}{4s+4} + \frac{(2s+1)!}{\left(-\frac{if\pi}{2d_1}\right)^{2s+2}}\right.$$

$$\left. - \exp\left(\frac{if\pi}{2}\right)\sum_{a=0}^{2s+1}\frac{(2s+1)!\;d_1^a}{a!\;\left(-\frac{if\pi}{2d_1}\right)^{2s+2-a}}\right] \quad (4\text{-}31)$$

Thus, substituting Eq. (4-29), (4-30) and (4-31) in Eq. (4-28) is the solution for $\langle E_2 \rangle$. Similarly, $\langle E_2{}^* \rangle$ is obtained by taking the conjugate of the expressions for I_1, I_2 and I_3, the detailed calculations are not repeated here.

$$\langle E_2^* \rangle = \left\langle \frac{W_x^* W_y^* E_{20} F}{T^2} e^{-\frac{1}{2}(\sigma V_z)^2} [I_1^* + I_2^* + I_3^*] \right\rangle_{\xi} \quad (4\text{-}32)$$

$D\{E_2\} = \langle E_2 E_2^* \rangle - \langle E_2 \rangle \langle E_2^* \rangle$ is the variance of the complex scattering field, it may be written (Beckman, 1963) in a form similar to Eq. (4-25) as

$$D\{E_2\} = \left\langle \frac{|W_x|^2 |W_y|^2 E_{20}^2 F^2}{T^4} \int_{-\frac{T}{2}}^{\frac{T}{2}}\int_{-\frac{T}{2}}^{\frac{T}{2}}\int_{0}^{2\pi}\int_{0}^{\infty} \exp[iV_x \tau \cos\phi + iV_y \tau \sin\phi + iV_z(\xi_1 - \xi_2)] \cdot [\Phi(V_z, -V_z) - \Phi(V_z)\Phi^*(V_z)] \tau \, d\tau \, d\phi \, dx_1 dy_1 \right\rangle_{\xi} \quad (4\text{-}33)$$

where

$$[\Phi(V_z, -V_z) - \Phi(V_z)\Phi^*(V_z)] = e^{-(\sigma V_z)^2} \sum_{m=1}^{\infty} \frac{(\sigma V_z)^{2m}}{m!} e^{-\frac{m\tau^2}{T^2}} \quad (4\text{-}34)$$

Let

$$K_1 = \frac{|W_x|^2 |W_y|^2 E_{20}^2 F^2}{T^4} \exp-(\sigma V_z)^2 \sum_{m=1}^{\infty} \frac{(\sigma V_z)^{2m}}{m!} \quad (4\text{-}35)$$

then

$$D\{E_2\} = \left\langle K_1 \int_0^{2\pi}\int_0^{\infty}\int_{-\frac{T}{2}}^{\frac{T}{2}}\int_{-\frac{T}{2}}^{\frac{T}{2}} \exp\left(\frac{-m\tau^2}{T^2}\right) \cdot \exp[iV_x \tau \cos\phi + iV_y \tau \sin\phi + iV_z(\xi_1 - \xi_2)] \, dx_1 dy_1 \tau \, d\tau \, d\phi \right\rangle_{\xi} \quad (4\text{-}36)$$

Also, let

$$I(\tau, \phi) = \int_{-\frac{T}{2}}^{\frac{T}{2}}\int_{-\frac{T}{2}}^{\frac{T}{2}} \exp[iV_z(\xi_1 - \xi_2)] \, dx_1 dy_1 \quad (4\text{-}37)$$

From the geometry of the periodic surface, it is observed that I (τ,ϕ) could be separated into three parts as (see Fig. 2-2):

$$I_1(\tau,\phi) = T^2 - \pi d_2^2 \tag{4-38}$$

$$I_2(\tau,\phi) = \iint_{Rim} \exp[iV_2(\xi_{p_1} - \xi_{p_2})]\, dx_1\, dy_1 \tag{4-39}$$

$$I_3(\tau,\phi) = \iint_{crater} \exp[iV_2(\xi_{p_1} - \xi_{p_2})]\, dx_1\, dy_1 \tag{4-40}$$

$$\left.\begin{aligned} \xi_{p_1} &= \xi_p(x_1, y_1) \\ \xi_{p_2} &= \xi_p(x_1 - \tau\cos\phi,\ y_1 - \tau\sin\phi). \end{aligned}\right\} \tag{4-41}$$

Now, performing the polar transformation for x_1, y_1 to r_1, θ, one obtains

$$x_1 = r_1 \cos\theta \tag{4-42}$$

$$y_1 = r_1 \sin\theta \tag{4-43}$$

$$dx_1\, dy_1 = |J|\, dr_1\, d\theta \tag{4-44}$$

$$|J| = \begin{vmatrix} \frac{\partial x_1}{\partial r_1} & \frac{\partial x_1}{\partial \theta} \\ \frac{\partial y_1}{\partial r_1} & \frac{\partial y_1}{\partial \theta} \end{vmatrix} = \begin{vmatrix} \cos\theta & -r_1\sin\theta \\ \sin\theta & r_1\cos\theta \end{vmatrix} = r_1 \tag{4-45}$$

where r_1 and r_2 are

$$r_1 = \sqrt{x_1^2 + y_1^2} \tag{4-46}$$

$$\begin{aligned} r_2 &= \sqrt{x_2^2 + y_2^2} \\ &= \sqrt{r_1^2 + \tau^2 - 2r_1\tau\cos(\theta - \phi)} \end{aligned} \tag{4-47}$$

the integral over Region II becomes

$$I_2(\tau,\phi) = \int_0^{2\pi}\int_{d_1}^{d_2} \exp\Big[iV_2h_2 \sin\frac{\pi(r_1-d_1)}{d_2-d_1} - iV_2h_2 \sin\frac{\pi(r_2-d_1)}{d_2-d_1}\Big]\, r_1\, dr_1\, d\theta$$

$$= \int_0^{2\pi}\int_{d_1}^{d_2} \exp\Big[i V_2 h_2 \sin \frac{\pi(R_1 - d_1)}{d_2 - d_1}$$

$$- i V_2 h_2 \sin \frac{\pi\left(\sqrt{R_1^2 + \tau^2 - 2R_1\tau\cos(\theta-\phi)} - d_1\right)}{d_2 - d_1}\Big] R_1\, dR_1\, d\theta \qquad (4-48)$$

After making an expansion of the exponential in Bessel functions, I_2 becomes

$$I_2(\tau,\phi) = \sum_{\mu=-\infty}^{\infty}\sum_{\nu=-\infty}^{\infty} J_\mu(V_2h_2)\, J_\nu(-V_2h_2)\, \exp\left[\frac{-i(\mu+\nu)\pi d_1}{d_2 - d_1}\right] \cdot$$

$$\int_0^{2\pi}\int_{d_1}^{d_2} \exp\left[\frac{i\pi\mu R_1}{d_2-d_1}\right] \cdot \exp\left[\frac{i\pi\nu}{d_2-d_1}\sqrt{R_1^2+\tau^2-2R_1\tau\cos(\theta-\phi)}\right] R_1\, dR_1\, d\phi \qquad (4-49)$$

The origin of the reference coordinates is chosen at the center of the crater such that the integral around the rim and the crater is symmetrical to ϕ; therefore, I_2 and I_3 are functions only of τ as given below:

$$I_2(\tau) = \sum_{\mu=-\infty}^{\infty}\sum_{\nu=-\infty}^{\infty} J_\mu(V_2h_2)\, J_\nu(-V_2h_2)\, \exp\left[\frac{-i(\mu+\nu)\pi d_1}{d_2 - d_1}\right]$$

$$\int_0^{2\pi}\int_{d_1}^{d_2} \exp\left[\frac{i\mu\pi R_1}{d_2-d_1}\right] \cdot \exp\left[\frac{i\nu\pi}{d_2-d_1}\sqrt{R_1^2+\tau^2-2R_1\tau\cos\theta}\right] R_1\, dR_1\, d\theta$$

$$= K_2\left(d_2^{a+l+2n+2} - d_1^{a+l+2n+2}\right)\tau^{b-2n} \qquad (4-50)$$

where

$$K_2 = \sum_{\mu=-\infty}^{\infty}\sum_{\nu=-\infty}^{\infty} J_\mu(V_2h_2)\, J_\nu(-V_2h_2)\, \exp\left[\frac{-i(\mu+\nu)\pi d_1}{d_2 - d_1}\right] \cdot$$

$$\sum_{l=0}^{\infty}\frac{1}{l!}\left[1-(-1)^{l+1}\right]\left[\frac{-i\nu\pi}{d_2-d_1}\right]^l \sum_{a=0}^{\infty}\sum_{b=0}^{\infty}\frac{1}{a!\,b!}$$

$$\left[\frac{i\pi}{d_2-d_1}\right]^{a+b} \mu^a\, \nu^b\; B(a+l+2,\ 1)$$

$$\sum_{n=0}^{\infty}(-1)^n \frac{\left(\frac{l-b}{2}\right)_n \left(\frac{a+l+2}{2}\right)_n}{n!\left(\frac{a+l+4}{2}\right)_n} \qquad (4-51)$$

with B(x,y), the beta function, given by

$$B(x,y) = \int_0^1 t^{x-1}(1-t)^{y-1}\,dt \qquad (4\text{-}52)$$

and $(X)_n$, the hypergeometric series, given by

$$(x)_n = x(x+1)(x+2)\cdots(x+n-1) \qquad (4\text{-}53)$$

The integral over Region III (the crater) is

$$I_3(r) = \iint_{crater} \exp\left[iV_2(\xi_{p_1} - \xi_{p_2})\right] dx_1\,dy_1 \qquad (4\text{-}54)$$

A transformation similar to that for I_2 yields the following value for I_3

$$I_3(r) = \int_0^{d_1}\int_0^{2\pi} \exp\left[-iV_2 h_1 \cos\frac{\pi r_1}{2d_1} + iV_2 h_1 \cos\frac{\pi r_2}{2d_1}\right] r_1\,dr_1\,d\theta \qquad (4\text{-}55)$$

A substitution of

$$r_2 = \sqrt{r_1^2 + r^2} - \frac{r_1 r}{\sqrt{r_1^2 + r^2}} \cos\theta \qquad (4\text{-}56)$$

into I_3 above yields

$$I_3(r) = \sum_{\mu=-\infty}^{\infty}\sum_{\nu=-\infty}^{\infty} (i)^{\mu+\nu} J_\mu(-V_2 h_1)\, J_\nu(V_2 h_1)$$

$$\int_0^{d_1} \exp\left[\frac{i\mu\pi r_1}{2d_1} + \frac{i\nu\pi}{2d_1}\sqrt{r_1^2 + r^2}\right]$$

$$\int_0^{2\pi} \exp\left[\frac{-i\nu\pi}{2d_1}\frac{r_1 r}{\sqrt{r_1^2 + r^2}}\cos\theta\right] d\theta\, r_1\,dr_1 \qquad (4\text{-}57)$$

which integrated, yields

$$I_3(r) = K_3\, d_1^{\,m+l+2n+2}\, r^{\,b-2n} \qquad (4\text{-}58)$$

where

$$K_3 = \sum_{\mu=-\infty}^{\infty}\sum_{\nu=-\infty}^{\infty} (i)^{\mu+\nu} J_\mu(-V_2 h_1)\, J_\nu(V_2 h_1)\cdot$$

$$\sum_{\ell=0}^{\infty} \frac{1}{\ell!} \left[\frac{-i\nu\pi}{2d_1} \right]^{\ell} \left[1-(-1)^{\ell+1} \right] \sum_{a=0}^{\infty} \sum_{b=0}^{\infty} \frac{1}{a!\, b!}$$

$$\left[\frac{i\pi}{2d_1} \right]^{a+b} \mu^a \nu^b \quad B(a+\ell+2, 1)$$

$$\sum_{n=0}^{\infty} (-1)^n \frac{\left(\frac{a-b}{2}\right)_n \left(\frac{a+\ell+2}{2}\right)_n}{n! \left(\frac{a+\ell+4}{2}\right)_n} \qquad (4-59)$$

$$D\{E_2\} = \left\langle K_1 \int_0^{2\pi}\int_0^{\infty} \exp\left(\frac{-m\tau}{B}\right) \cdot \exp(iV_x\tau\cos\phi + iV_y\tau\sin\phi) \cdot \right.$$

$$\left. [I_1 + I_2 + I_3]\ \tau\, d\tau\, d\phi \right\rangle_{\xi_p} \qquad (4-60)$$

But

$$\int_0^{2\pi} \exp(iV_x\tau\cos\phi + iV_y\tau\sin\phi)\, d\phi \simeq 2\pi J_0\left(\tau\sqrt{V_x^2+V_y^2}\right) \qquad (4-61)$$

$$D\{E_2\} = \left\langle K_1\, 2\pi \int_0^{\infty} \exp\left(\frac{-m\tau}{B}\right) J_0\left(\tau\sqrt{V_x^2+V_y^2}\right) \right.$$

$$\left. [I_1 + I_2 + I_3]\ \tau\, d\tau \right\rangle_{\xi_p}$$

$$= \left\langle 2\pi K_1 [I_1' + I_2' + I_3'] \right\rangle_{\xi_p} \qquad (4-62)$$

where

$$I_1' = (T^2 - \pi d_2^2) \int_0^{\infty} \exp\left(\frac{-m\tau}{B}\right) J_0\left(\tau\sqrt{V_x^2+V_y^2}\right) \tau\, d\tau$$

$$= (T^2 - \pi d_2^2) \frac{\frac{m}{B}}{\left[\left(\frac{m}{B}\right)^2 + V_x^2 + V_y^2\right]^{3/2}} \qquad (4-63)$$

$$I_2' = K_2 \left[d_2^{a+\ell+2n+2} - d_1^{a+\ell+2n+2} \right] \int_0^{\infty} \exp\left(\frac{-m\tau}{B}\right) \cdot$$

$$J_0\left(\tau\sqrt{V_x^2+V_y^2}\right) \tau^{b-2n+1}\, d\tau$$

$$= K_2 \left[d_2^{\,a+l+2n+2} - d_1^{\,a+l+2n+2} \right] (-1)^{b-2n+1}$$

$$\frac{\partial^{(b-2n+1)}}{\partial \left(\frac{m}{B}\right)^{(b-2n+1)}} \left[\frac{1}{\left(\frac{m^2}{B^2} + V_x^2 + V_y^2\right)^{1/2}} \right], \text{ AND} \qquad (4\text{-}64)$$

$$I_3' = K_3 \; d_1^{\,a+l+2n+2} \int_0^\infty \exp\left(-\frac{m\tau}{B}\right) J_0\left(\tau\sqrt{V_x^2+V_y^2}\right) \tau^{b-2n+1} \, d\tau$$

$$= K_3 \, d_1^{\,a+l+2n+2} (-1)^{b-2n+1} \frac{\partial^{(b-2n+1)}}{\partial \left(\frac{m}{B}\right)^{(b-2n+1)}} \left[\frac{1}{\left(\frac{m^2}{B^2} + V_x^2 + V_y^2\right)^{1/2}} \right]$$

$$(4\text{-}65)$$

The solution is

$$D\{E\} = \left\langle K_1 \, 2\pi \left[I_1' + I_2' + I_3' \right] \right\rangle_{S_T} \qquad (4\text{-}66)$$

The complete solution described in Eq. (4-26) is the product of Eq. (4-28), (4-32) plus (4-66).

The solution obtained above for the two dimensional scattering from the lunar surface is valid for all points in space. The monostatic radar where the parameters in $\langle E_2 E_2^* \rangle$ are

$$\theta_2 = -\theta_1 \qquad (4\text{-}67)$$

$$\theta_3 = 0 \qquad (4\text{-}68)$$

$$F = \frac{1}{\cos^3\theta_1} \qquad (4\text{-}69)$$

$$|W_y|^2 = 1 \qquad (4\text{-}70)$$

$$V_y = 0 \qquad (4\text{-}71)$$

$$|W_x|^2 = \left(\frac{\sin 2n\rho\pi}{2n \sin \rho\pi} \right)^2 \quad (4\text{-}72)$$

$$V_x = \frac{4\pi}{\lambda} \sin\theta_1 \quad (4\text{-}73)$$

$$V_z = -\frac{4\pi}{\lambda} \cos\theta_1 \quad (4\text{-}74)$$

$$n = \frac{L_x}{T} \quad (4\text{-}75)$$

$$\rho = \frac{2T}{\lambda} \sin\theta_1 \quad (4\text{-}76)$$

The final solution of the radar return power $\langle E_2 E_2^* \rangle$ is expressed in terms of a set of conditions and terrain parameters. The radar antenna orientation with respect to the surface normal is substituted for θ_1; V_x and V_z and W_x is thus determined accordingly. The variance σ and the correlation distance B are the random surface characteristics, and may assume different values which can be fitted for the description of a certain section along the LM approach. The variables h_1, h_2, d_1, and d_2 are linear functions of D, the crater diameter, which is a random variable with an independent probability density function p(d) which is nonuniform over the whole landing track. However, p(d) may be approximated to be piecewise uniform. Thus, with the aid of the computer, the required radar return degradation curve can also be calculated.

CHAPTER V

CONCULSION

A very realistic lunar surface model description using a superposition of a sinusoidal quasi-periodic component and a randomly rough component surface is presented. This model is believed to represent lunar surface conditions and the regularly existing rough features such as craters, hills and boulders as shown by the Surveyors and Orbitors photographs

The solution of the radar signal return based on this new model is calculated using the scalar Helmholtz Integral. The result is verified for various conditions such as when the random component or the quasi-periodic component or both become zero, respectively. In all cases it is found that the result checks well with the work reported previously in the literature by other authors.

The one-dimensional and the two-dimensional radar return calculations are included with their implications. The scattering from a short range radar, where the beam cross-section area is small compared to the dimensions of the surface, the one-dimensional solution is appropriate and moreover its evaluation is simple, whereas for long range radar return it is necessary to use the two-dimensional solution. One must employ a spherical wave instead of a plane wave for very low altitude return.

The superposition of one or more quasi-periodic and random components as used for the lunar surface modeling may be extended to model several other types of terrain.

BIBLIOGRAPHY

Beckman, P. and A. Spizzichino. The Scattering of Electromagnetic Waves From Rough Surfaces. New York: The MacMillan Co., 1963.

Bobrovnikoff, N. T. Natural Environment of the Moon: WADC Phase Technical Note 3. Ohio State University Research Foundation, June, 1959.

Born and Wolf. Principles of Optics. New York: Pergamon Press, 1964.

Brunschwig, M., et al. Estimation of the Physical Constants of the Lunar Surface. The University of Michigan, November, 1960.

Claxton, Brian H. and Roy E. Anderson. Lunar Reflection Study. Contract No. AF19(604)-6634, Final Report, Part II, August 31, 1962.

Daniels, Fred B. A Theory of Radar Reflection from the Moon and Planets (publication pending)

Evans, J. V. Radio-Echo Observations of the Moon at 3.6cm Wavelength. Lincoln Laboratory, Mass. Inst. of Tech., Tech. Rept. No. 256, August 30, 1960.

Evans, J. V., et al. Radio-Echo Studies of the Moon at 7.84 Meter Wavelength. Lincoln Laboratory, Mass. Inst. of Tech., Tech. Rept. No. 288, November 20, 1962.

Fung, A. K. "Theory of Radar Scatter from Rough Surfaces, Bistatic and Monostatic, with Application to Lunar Radar Return," Journal of Geophysical Research, Vol. 69, No. 6 (March, 1964), 1063-1072.

Hayre, H. S. "Radar Back-Scatter Theories for Near-Vertical Incidence and Their Application to an Estimation of the Lunar Surface Roughness." Engineering Exp. Station, University of New Mexico, Albuquerque, Ph.D. Dissertation Rept. No. EE-67, January, 1962.

Hayre, H. S. and D. E. Kaufman. "Plane Wave Scattering from a Rough Surface with Correlated Large and Small Scale Orders of Roughness," The Journal of the Acoustic Society of America, Vol. 38, No. 4 (October, 1965), 599-603.

Hayre, H. S. "Acoustic Simulation of Lunar Echoes," Journal of Geophysical Research, Vol. 70, No. 16 (August 15, 1965), 3831-3839.

Hayre, H. S. "Surface Roughness of the Moon," Journal of the British Interplanetary Society, Vol. 13, No. 10 (August, 1962), 389-391.

Hayre, H. S. "Statistical Methods in Radar Astronomy. Determination of Surface Rougnness," Journal of Research of the National Bureau of Standards - D. Radio Propagation, Vol. 67D, No. 6 (November-December, 1963), 763-764.

Hayre, H. S. and R. K. Moore. "Theoretical Scattering Coefficient for Near Vertical Incidence From Contour Maps," Journal of Research of the National Bureau of Standards - D. Radio Propagation, Vol. 65D, No. 5 (September-October, 1961), 427-432.

Herriman, A. G., et al. Ranger Preflight Science Analysis and the Lunar Photometric Model. Tech. Rept. No. 32-384, California Inst. of Tech., January 7, 1963.

Irving, J. and N. Mullineaux. Mathematics in Physics and Engineering. New York: Academic Press, 1959.

Jackson, J. D. Classical Electrodynamics. New York: John Wiley and Sons, Inc., 1962.

Lindsey, R. B. Mechanical Radiation. New York: McGraw Hill, 1960.

Metzner, Albert E. An X-Ray Spectograph for Lunar Surface Analysis. Tech. Rept. No. 32-669, California Inst. of Tech., October 16, 1964.

Middleton, D. An Introduction to Statistical Communication Theory. New York: McGraw-Hill, 1960.

Muhleman, D. O. "Radar Scattering from Venus and the Moon, Astron. J., Vol. 69 (1964), 34-41.

"Paris Symposium on Radio Astronomy," Proceedings of the 1958 IAU-URSI Symposium, Stanford University, 1959.

Reza, Fazlollah M. An Introduction to Information Theory. New York: McGraw-Hill, 1961.

"Screen Report of Lunar Orbiter II Photography at NASA-Langley Research Center," for NASA Manned Spacecraft Center, Houston, 1967.

Speed, Robert C., et al. A Lunar X-Ray Diffraction Experiment. NASA Tech. Rept. No. 32-756, California Inst. of Tech., September 1, 1965.

"Surveyor I Mission Report," Jet. Prop. Lab., Tech. Rept. 32-1023, Pasadena, California, September 10, 1966.

Stratton, J. A. Electromagnetic Theory. New York: McGraw-Hill, 1941.

"The Nature of the Lunar Surface," Proceedings of the 1965 IAU-NASA Symposium, Johns Hopkins University, Baltimore, 1966.

Willingham, D. The Lunar Reflectivity Model for Ranger Block III Analysis. Tech. Rept. No. 32-664, California Inst. of Tech., November 2, 1964.

Wolff, Edward A. Antenna Analysis. New York: John Wiley and Son, Inc., 1966.